

Cosmic ray modulation of infra-red radiation in the atmosphere

K L Aplin¹ and M Lockwood²

1. Physics Department, University of Oxford, Denys Wilkinson Building, Keble Road, Oxford OX1 3RH

2. Space and Atmospheric Electricity Group, Department of Meteorology, University of Reading, Earley Gate, Reading RG6 6BB

Corresponding author: k.aplin1@physics.ox.ac.uk

Abstract. Cosmic rays produce charged molecular clusters by ionisation as they pass through the lower atmosphere. Neutral molecular clusters such as dimers and complexes are expected to make a small contribution to the radiative balance, but atmospheric absorption by charged clusters has not hitherto been observed. In an atmospheric experiment, a filter radiometer tuned to the 9.15 μm absorption band associated with infra-red absorption of charged molecular clusters was used to monitor changes immediately following events identified by a cosmic ray telescope sensitive to high energy ($>400\text{MeV}$) particles, principally muons. The change in longwave radiation in this absorption band due to charged molecular clusters is 7 mWm^{-2} . The integrated atmospheric energy change for each event is 2J, representing an amplification factor of 10^{10} compared to the 2GeV energy of a typical tropospheric cosmic ray. This absorption is expected to occur continuously and globally.

Keywords

molecular clusters, atmospheric ions, ionisation, cosmic rays, infra-red radiation

PACS codes

92.60.Pw Atmospheric electricity, lightning

92.60.Vb Radiative processes, solar radiation

92.70.Qr Solar variability impact

95.85.Ry Neutrino, muon, pion, and other elementary particles; cosmic rays

1. Introduction

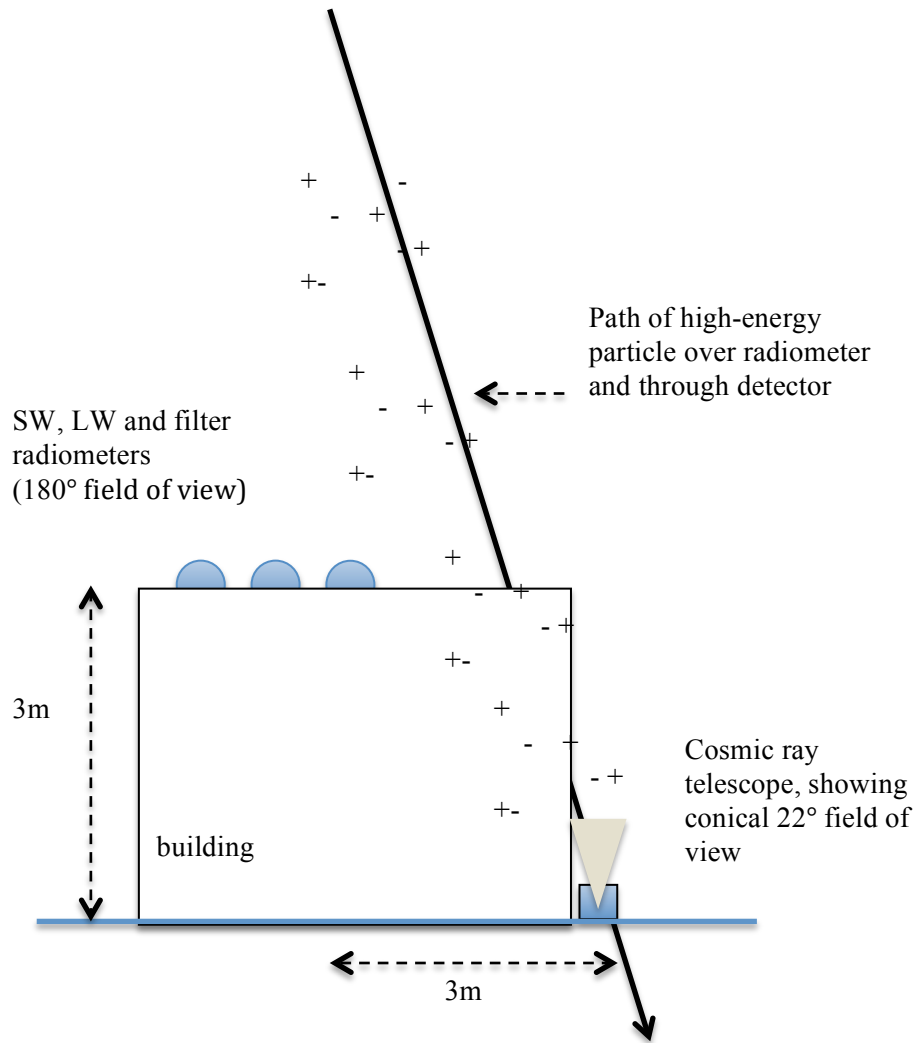
Atmospheric charged molecular clusters (CMC) are bipolar ionic species formed by ionisation from high-energy cosmic ray particles, mainly secondary GeV muons in the troposphere, and natural radioactivity. CMC are generated when core positive ions e.g. N_2^+ , or electrons become attached to electrophilic molecules (e.g. O_2^-), and rapidly cluster with polar ligands that are hydrogen bonded to the core ion e.g. $\text{HSO}_4^-(\text{H}_2\text{SO}_4)_m(\text{H}_2\text{O})_n$ or $\text{H}_3\text{O}^+(\text{H}_2\text{O})_n$ [1,2]. The wide range of hydrogen-bonded atmospheric CMC species absorb and emit infra-red (IR) radiation, for example IR transitions associated with bond stretching and bending for the gas phase protonated water dimer $\text{H}_3\text{O}^+(\text{H}_2\text{O})_2$ have been measured in the laboratory [3]. Although the contributions of neutral molecular clusters, such as the water oligomer $(\text{H}_2\text{O})_n$ and hydrated complexes (e.g. $\text{O}_2\text{-H}_2\text{O}$) to atmospheric radiative transfer via IR absorption are being actively investigated [4,5], the radiative properties of atmospheric CMC – which are a direct effect on the atmosphere's radiation budget - have not hitherto been considered. Responses of CMC to sudden decreases in cosmic rays have already been indirectly demonstrated through atmospheric electricity changes [2], but here we present evidence that CMC formed in the atmosphere by cosmic rays also absorb IR radiation within the broad absorption band previously identified in laboratory experiments.

1 Laboratory spectroscopy experiments using artificially generated CMC detected IR
2 absorption of 1-3% in two bands centred on 9.15 and 12.3 μm [6,7], with CMC columnar
3 concentrations of 10^{13} m^{-2} . As the atmospheric CMC columnar concentration is estimated to
4 be 10^{14} m^{-2} , detectable absorption from atmospheric CMC is therefore expected. Based on
5 these laboratory data, the experiment described in this paper was devised to search for the
6 effects of atmospheric CMC on longwave radiation. In this paper we report the atmospheric
7 response of a filter radiometer tuned to the 9.15 μm CMC absorption band, following cosmic
8 ray events ionising the atmospheric column above the radiometer.
9

10 2. Experiment

11
12 The sensor used in this experiment was an atmospheric filter radiometer tuned to pass
13 radiation in the region centred upon 9.15 μm with a bandwidth (FWHM) of 0.9 μm (i.e $\pm 5\%$
14 of band centre) [8], with a stable low noise amplifier [9] for signal conditioning. A small
15 cosmic ray telescope was located close to the filter radiometer, to detect the high-energy
16 particles [10] creating atmospheric CMC over the radiometer. Adjacent broadband
17 radiometers were used to monitor downwelling atmospheric short wave (SW, 0.3-3 μm)
18 radiation, emitted by the Sun, and downwelling, terrestrially emitted, long wave (LW, 4.5-42
19 μm) radiation. The cosmic ray telescope indicates an “event” when both its detectors are
20 triggered by high-energy particles travelling down through the atmosphere (the false
21 triggering rate has been shown to be negligible [10]). Subsidiary experiments were carried out
22 to investigate the energy sensitivity of the detector by placing it beneath varying quantities of
23 lead and concrete, selected to absorb different energies of particle [e.g. 11]. These showed
24 that the telescope responds to particles with energy $>400 \text{ MeV}$, which, at the surface, are
25 almost all muons (mean energy 2GeV) [12]. The detectors (Figure 1) were arranged
26 geometrically to prevent a high-energy particle from passing through both the radiometer
27 amplifier and the cosmic ray telescope, reducing the possibility of cross-talk between the
28 instruments. Previous experiments with the same apparatus showed, firstly, the electrical
29 conductivity of the air, which is approximately proportional to the atmospheric CMC
30 concentration, increased after muon events [13]. Secondly, the filter radiometer employed
31 here has already been shown to respond to changes in atmospheric CMC concentration in a
32 calibration experiment using direct measurements of CMC [14].
33

34 The cosmic ray telescope was housed in a waterproof enclosure at a semi-rural UK site
35 (51.8929N, 2.1300W). The filter radiometer was installed above it on a nearby rooftop,
36 adjacent to the broadband radiometers of a Kipp and Zonen CNR1 instrument. A Campbell
37 CR3000X data logger was used to count the cosmic ray telescope events and to log the
38 radiometer data. Data were averaged over 20s, which is the timescale for the radiometer to
39 fully respond to a step change. The 20s data samples were only saved for 200s either side of a
40 triggering event, and 5 minute averages were also recorded. The experiment ran from July
41 2008 to June 2009, over which the mean high-energy particle flux was $33 \text{ m}^{-2}\text{ster}^{-1}\text{s}^{-1}$,
42 consistent with the mean flux of $>1\text{GeV}$ muons expected at the surface [12].

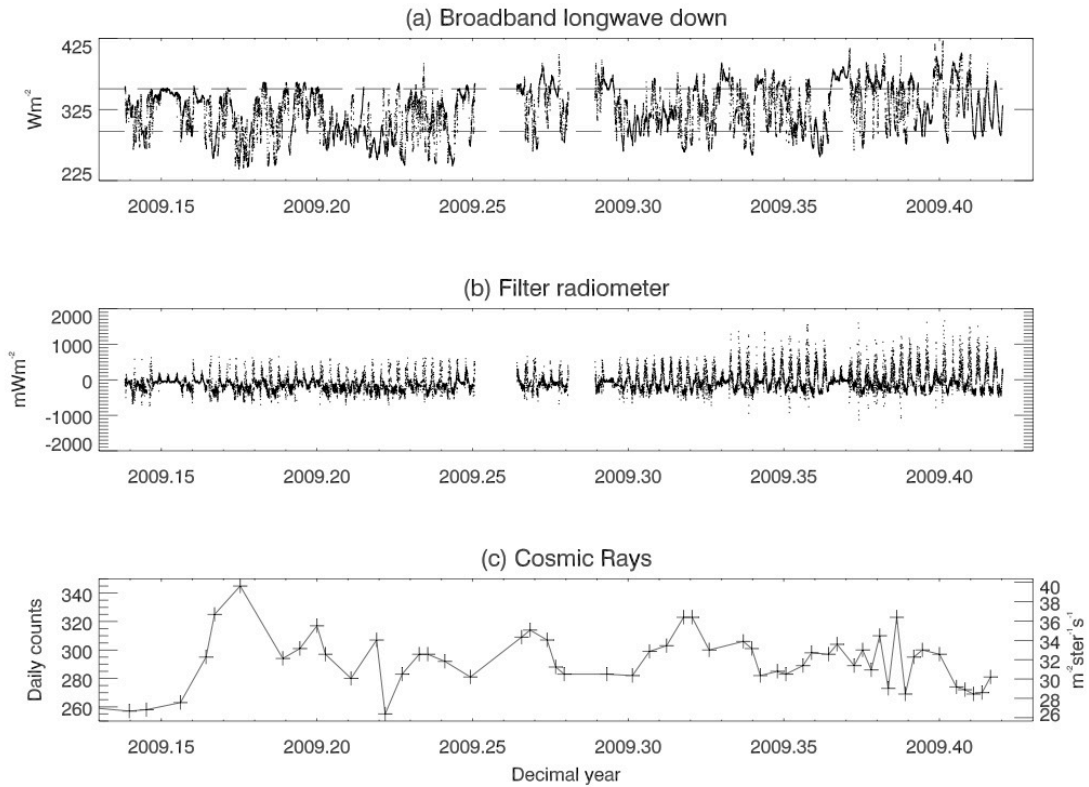


1
2
3
4
5
6
7
8
9
10
11
12
13
14
15
16
17
18
19
20
21

Figure 1 Schematic arrangement of the experiment, (not to scale) showing the radiometers mounted on a building and the adjacent cosmic ray telescope. The telescope can detect particles in a cone 11° from the vertical, with the geometry implying that approximately half the particles detected have passed over the radiometer at a height of >15m.

3. Results

The IR radiation measured by the filter radiometer is calibrated with reference to the blackbody atmospheric brightness temperature in its passband, calculated with data from the CNR1 LW radiometer [15]. A positive response from the filter radiometer indicates emission in the CMC wavelength range in the column above the radiometer, and a negative signal indicates absorption with respect to the blackbody background. Figure 2 shows a time series of the combined data from all instruments for approximately six months in 2009. The typical variations in each quantity can be seen, particularly the range in LW down, which is greatest in warm, cloudy skies and least in the nocturnal clear sky. The filter radiometer output shows a diurnal variation, with more absorption in the band at night and more emission during the day.



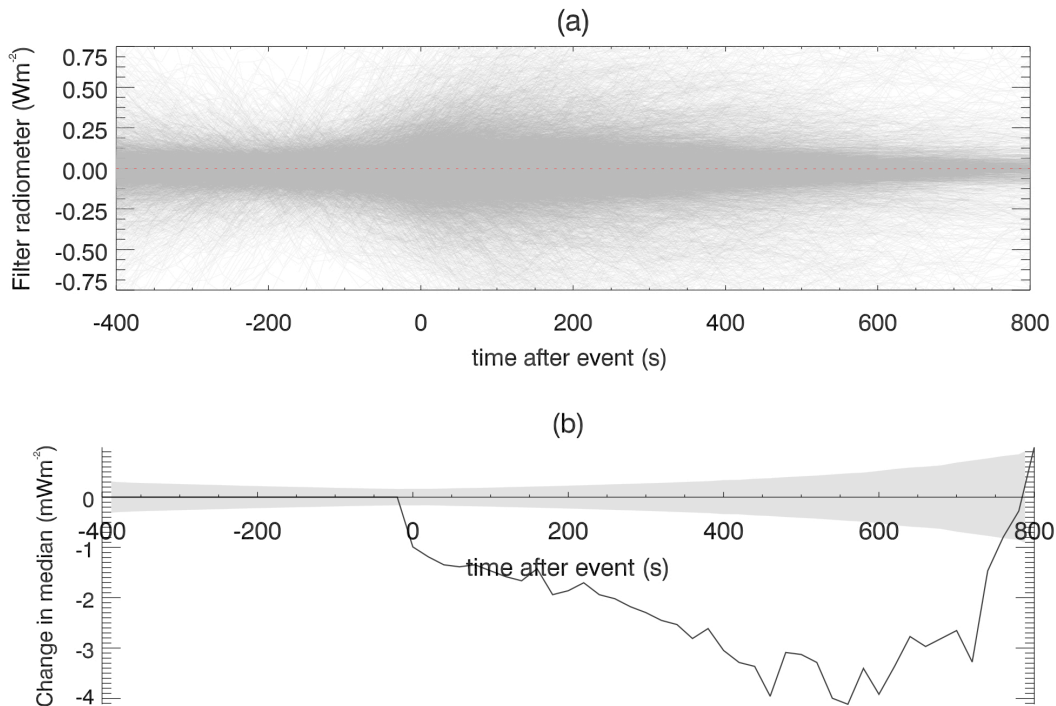
1
2 Figure 2 Time series of typical data, from 16th February – 6th June 2009 showing (a) broadband
3 longwave down (5 minute averages) with the upper ($354\ Wm^{-2}$) and lower ($295\ Wm^{-2}$) quartiles as
4 horizontal dashed lines (b) filter radiometer signal (5 minute averages). (c) daily averages of the raw
5 muon flux, not temperature or pressure corrected, shown as both daily counts (left hand axis) and flux
6 (right hand axis).

7
8 The data analysis approach taken is to separate out the response around each cosmic ray
9 telescope event, which are averaged together (“composited”) to obtain the typical response.
10 Compositing many events (also referred to as a “superposed epoch” or a “Chree” analysis) is
11 a well-established technique for extracting signals despite background variability when there
12 is a known triggering event [16]. Although the atmospheric pressure and temperature do
13 affect the surface muon flux [17,18] plotted here as raw data in figure 2(c), our compositing
14 approach means that we only analyse the immediate change in the local radiative response to
15 individual particles on timescales which are much shorter than the pressure and temperature
16 changes (which would average out in the analysis in any case).

17

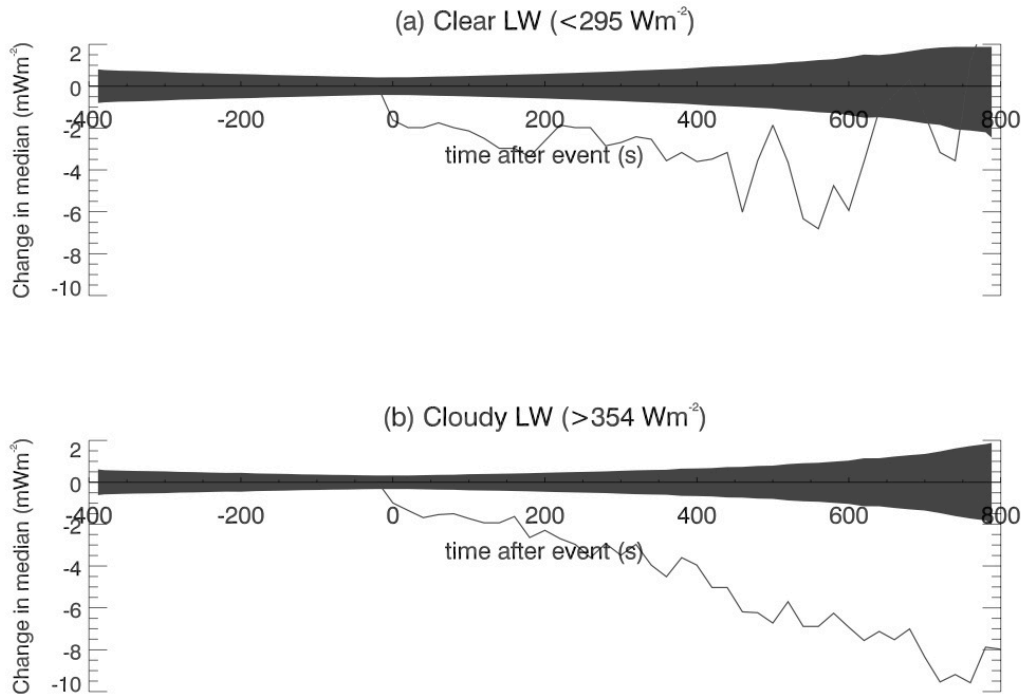
1 **3.1 Compositing data**

2
 3 Figure 3a shows infra-red changes measured by the filter radiometer from 25th July 2008 to
 4 2nd June 2009, plotted as a composite around each high-energy particle event (which occurs at
 5 time $t = 0$ in each case). All the available data has been used to form the composite, with each
 6 event normalised by subtracting the median infra-red absorption in the 400s before the event.
 7 A difference in response before and after the event can be seen to emerge through the
 8 variability. In figure 3b the median of the response in figure 3a is compared to numerous
 9 realisations of randomised data chosen from the period before each event, for the same
 10 number of random points as the number of filter radiometer data points at each sample. The
 11 median response to all events shows a statistically significant absorption of up to 4 mWm^{-2} ,
 12 which then recovers to the pre-event level.



13
 14
 15 Figure 3 Compositing infra-red filter radiometer data from 25th July 2008 to 2nd June 2009, showing
 16 atmospheric absorption in the $9.15 \pm 0.45 \mu\text{m}$ band. Data is plotted as a function of time, triggered on
 17 each high-energy particle event at 0s. If another event occurs within 800s, only data until just before
 18 the next event is included. The response to 31398 events is shown, with the median subtracted in the
 19 400s before each event. (a) Time series for each event (grey lines), with the median of all points at each
 20 sample time shown as a red dotted line. (b) Change in median filter radiometer signal following each
 21 event (grey line). The shaded region indicates the natural variability expected for the number of points
 22 in the composite, determined from periods during which no high-energy particle events were recorded.
 23 The pre-event variability is calculated from the usual confidence range on the median for a non-
 24 Gaussian distribution ($1.58 \times$ the interquartile range divided by the square root of the number of points
 25 [19]).

26
 27 As the IR radiation emitted by water vapour in cloud will contribute to the filter radiometer
 28 signal, one expectation might be that the direct IR absorption of CMC is most apparent in
 29 clear sky. In cloudy sky, the additional small absorption from background water vapour
 30 would contribute, and could obscure the absorption effect. Situations in which clouds are
 31 largely absent are chosen by selecting the lower quartile of the LW measurements. The lower
 32 quartile ($\text{LW} < 295 \text{ Wm}^{-2}$) is dominated by measurements on clear winter nights, whereas the
 33 upper quartile ($\text{LW} > 354 \text{ Wm}^{-2}$) occurs mainly under cloudy conditions in the spring.



1
2 Figure 4 Change in median filter radiometer output (similar to figure 3b), sorted by downwelling
3 longwave radiation (a) lower quartile ($<295 \text{ Wm}^{-2}$), 6295 events (c) upper quartile ($>354 \text{ Wm}^{-2}$), 8164
4 events. The shaded region indicates the natural variability expected for the number of points in the
5 composite, determined from periods during which no high-energy particle events were recorded (as for
6 figure 3).

7
8 The two situations are compared in Figure 4. This indicates that the same sign of response is
9 apparent in both cloudy and clear skies, with the absorption appearing both more enhanced,
10 and of longer duration in cloudy skies (Figure 4b) compared to clear, cold skies (Figure 4a).
11 The apparent enhancement of magnitude of the effect in cloudy sky is likely to be related to
12 background water vapour absorption in the passband.

13 14 3.2 Timescale of the effect

15
16 If the absorption seen is a response to ionisation above the radiometer caused by cosmic rays,
17 then the shape of the response should reflect the physics of atmospheric CMC. The
18 observations are consistent with increased ionisation after the events, followed by a recovery
19 as the CMC are lost by attachment to atmospheric aerosol particles or self-recombination.

20
21 The recombination losses of CMC will be considered first, which are hypothesised to cause
22 the recovery back to pre-event conditions from the IR minimum shown in Figure 3(b). In
23 relatively clean air, recombination of oppositely charged CMC dominates and the CMC
24 lifetime t_r is given by

$$25 \quad t_r = \frac{1}{\alpha n} \quad (1)$$

26 where α is the recombination coefficient ($1.6 \times 10^{-6} \text{ cm}^3 \text{ s}^{-1}$ for typical surface conditions [1])
27 and n is the CMC concentration. Using the differential of a spline fitted to the data to identify
28 the minimum gives a recovery period of $(280 \pm 60) \text{ s}$. Using (1) to estimate the CMC
29 concentration from the recovery time gives $n = (2300 \pm 500) \text{ cm}^{-3}$, which is consistent with
30 slightly enhanced CMC concentrations over typical measured background levels [1], as
31 expected from a burst of CMC created by the high-energy particle.
32

1 The initial slow linear increase in absorption following the cosmic ray event trigger occurs
2 over (520 ± 60) s. As the high-energy particles are relativistic, and initial ionisation occurs over
3 nanoseconds, this will be related to the spread of the CMC in the atmosphere above the
4 radiometer. From the experiment geometry (Figure 1), any particle triggering the telescope
5 must pass directly over the radiometer at a height of at least 15m, and will form CMC only
6 around its track. The absorption effect seen can be explained by fresh CMC drifting towards
7 the radiometer after a burst of ionisation. The IR absorption then slowly returns to pre-event
8 levels as the CMC are lost by recombination. Mobility μ , defined in equation (2), can be used
9 to determine the drift speed v attained by charged clusters in an electric field of magnitude E
10 as

$$v = \mu E \quad (4).$$

11
12 As the typical atmospheric electric field is 100 Vm^{-1} , and is downwards directed, then the
13 positive CMC formed will drift downwards, and the negative CMC upwards at 1 cms^{-1} ,
14 moving $\sim 5\text{m}$ in 500s. In comparison, molecular diffusion would be negligible in the time
15 considered, and advection by the wind would distribute the CMC over at least 100m.

16 17 **4. Discussion**

18 19 20 **4.1 Sources of variability**

21
22 The cosmic ray telescope detects high-energy particles in a solid angle of 0.34 steradians from
23 the vertical, whereas the radiometer responds to changes over almost a hemisphere (2π
24 steradians). The radiometer is therefore affected by local clouds and water vapour over a solid
25 angle twenty times greater than the muon detector. This will cause background variability in
26 the radiometer signal unrelated to ionisation, and may explain why many events need to be
27 composited to see an effect. Because there is a cascade of secondary particles from one
28 primary cosmic ray particle (an “air shower”), CMC can be formed in the radiometer field of
29 view by particles not travelling in the acceptance cone of the telescope. Some cosmic rays
30 will also pass through the telescope without passing over the radiometer. If the IR-CMC
31 absorption is caused by air showers generating CMC over an area, this would also mean many
32 events were needed to see a signal, when triggering on only those muons within the narrow
33 acceptance cone of the telescope. This could be readily confirmed by experiments with
34 separated cosmic ray detectors, which are often co-located with detailed meteorological
35 measurements [e.g. 18,20].

36 37 **4.2 Radiative contribution**

38
39 In estimating the radiative forcing caused by GCRs, it is important to bear in mind that the
40 effect seen has only been measured in the passband and could also be occurring in other
41 spectral regions, e.g the $12.3\mu\text{m}$ band seen in the laboratory [6]. Thus the radiative effect
42 evaluated here is expected to be an underestimate.

43
44 The events used to form the composites shown in figures 3 and 4 occurred at an average rate
45 of 12 hr^{-1} and the additional IR absorption averaged $\sim 2.5 \text{ mWm}^{-2}$ over 800 s. Therefore the
46 average power trapped (radiative forcing) is $2.5 \times 12 \times 800 / (60 \times 60) \sim 7 \text{ mWm}^{-2}$. The
47 observations presented were made in 2008-2009, during the deepest and longest-lived
48 minimum in solar activity since about 1920 [21], giving an unprecedented maximum in the
49 cosmic ray counts. The lowest count rates seen by neutron monitors at mid geomagnetic
50 latitudes, during large Forbush decreases at sunspot maxima in the modern era, are typically
51 60% of the peak value seen during the recent solar minimum. Thus we expect the solar
52 modulation of cosmic rays to induce a variation of up to 40% of this radiative forcing of 7
53 mWm^{-2} i.e. $\sim 3 \text{ mWm}^{-2}$. Reconstructions of the long-term variation in cosmic ray fluxes give
54 centennial-scale variations on of the same order as the solar cycle changes discussed above

1 [22,23] and hence we expect changes in decadal mean forcing also to be only about 3mWm^{-2} .
2 This is a small forcing compared to other known factors: for example the change in trace
3 greenhouse gas concentrations over the past century gives about 2.5Wm^{-2} and the estimated
4 change in total solar irradiance gives a radiative forcing of about 0.2Wm^{-2} [21]. Our results,
5 which represent the first quantification of this effect in the atmosphere, allow us to conclude
6 that this is unlikely to be a significant factor modulating Earth's energy balance, although it is
7 expected to occur both globally and continuously.

8
9 However, in terms of each muon event, the integrated energy transfer is 1.9 J. As the typical
10 energy of a muon is 2GeV (10^{10}J), the radiative change provides a substantial energy
11 amplification, of 10^{10} . This is direct, in comparison to other proposed mechanisms for
12 radiative effects of cosmic rays [24]. Finally, an interesting point arises from these results in
13 terms of monitoring cloud cover from space. The attenuation of the outgoing longwave
14 radiation is used in retrieval algorithms to determine cloud cover in remote sensing data.
15 Hence, using the passband of our experiment to derive low cloud from satellite data [25 and
16 references therein] could contribute to a solar imprint in observations of satellite-derived
17 global cloud cover.

18 **Acknowledgements**

19
20
21 This work was partially funded by the UK Science and Technology Facilities Council. We
22 thank Prof R.G. Harrison (Reading University) and Prof T Sloan (Lancaster University) for
23 helpful comments.

24 **References**

-
- 25
[1] R G Harrison and K S Carslaw, Ion-aerosol-cloud processes in the lower atmosphere
Reviews of Geophysics **41** (3), 1012, (2003)
[2] I Mironova et al, *Space Science Reviews*, submitted (2012)
[3] K Asmis et al, Gas-phase infrared spectrum of the protonated water dimer, *Science*, 299,
1375-1377 (2003)
[4] W Klemperer and V Vaida, Molecular complexes in close and far away, *PNAS* 1-3, 28,
10584-10588 (2006)
[5] K P Shine et al, The water vapour continuum: brief history and recent developments,
Surveys in Geophysics doi 10.1007/s10712-011-9170-y (2012)
[6] H R Carlon, Infrared absorption and ion content of moist atmospheric air, *Infrared*
Physics 22, 43-49 (1982)
[7] K L Aplin and R A McPheat, Absorption of infra-red radiation by atmospheric molecular
cluster-ions, *J. Atmos. Sol-Terr. Phys.*, 67, 775-783 (2005)
[8] K L Aplin and R A McPheat, An infra-red filter radiometer for atmospheric cluster-ion
detection, *Rev. Sci. Instrum* 79, 106107 (2008)
[9] R G Harrison and J R Knight, Thermopile radiometer signal conditioning for surface
atmospheric radiation measurements *Rev Sci Instrum* **77**, 116105 (2006)
[10] K L Aplin and R G Harrison, Compact cosmic ray detector for unattended atmospheric
ionization monitoring, *Rev Sci Instrum*, **81**, 124501 (2010)
[11] W B Gilboy et al, Muon radiography of large industrial structures, *Nuc. Inst. Meth. Phys.*
Res. B. **263**, 317-319 (2007)
[12] K Nakamura et al (Particle Data Group) 2011 Review of particle physics, *J. Phys G.* 37,
075021 (2011)
[13] R G Harrison and K L Aplin, Atmospheric condensation nuclei formation and high-
energy radiation *J. Atmos. Solar-Terrestrial Physics* **63**, 17, 1811-1819 (2001)
[14] K L Aplin, Composition and measurement of charged atmospheric clusters *Space Sci*
Revs **137**, 1-4, 213-224 (2008)
[15] M J Rycroft et al, Global electric circuit coupling between the space environment and the
troposphere, *J. Atmos. Sol-Terr. Phys.*, doi: 10.1016/j.jastp.2012.03.015 (2012)

- [16] S E Forbush et al, Statistical procedures for test Chree analysis results, *Proc 17th Int. Cosmic Ray Conf.*, Paris, France, 4 pp 47-51 (1981)
- [17] A M Hillas, *Cosmic rays*, Pergamon Press, Oxford (1972)
- [18] P Adamson et al (MINOS Collaboration), Observations of muon intensity variation by season with the MINOS far detector, *Phys. Rev. D.*, **81**, 012001 (2010)
- [19] R McGill et al (1978) Variations of box plots. *The American Statistician* **32**, 12–16
- [20] B Keilhauer et al (2004), Impact of varying atmospheric profiles on extensive air shower observation: atmospheric density and primary mass reconstruction, *Astropart. Phys.* **22**, 249
- [21] M Lockwood (2010) Solar change and climate: an update in the light of the current exceptional solar minimum, *Proc. R. Soc. A*, 466 303-329, doi:10.1098/rspa.2009.0519
- [22] I G Usoskin et al., A physical reconstruction of cosmic ray intensity since 1610, *J. Geophys. Res.*, 107(A11), 1374, doi:10.1029/2002JA009343, 2002
- [23] F Steinhilber et al (2008), Solar modulation during the Holocene, *Astrophys. Space Sci. Trans.*, **4**, 1–6, doi:10.5194/astra-4-1-008.
- [24] B A Tinsley and G W Deen (1991), Apparent tropospheric response to MeV-GeV particle flux variations: a connection via electrofreezing of supercooled water in high-level clouds? *J. Geophys. Res.*, **96**, D12, 22,283-22,296, doi:10.1029/91JD02473
- [25] N D Marsh and H Svensmark (2000), Low cloud properties influenced by cosmic rays, *Phys. Rev. Lett.* **85**, 23, 5004-500